AIAA AVIATION Forum
17-21 June 2019, Dallas, Texas
AIAA Aviation 2019 Forum

10.2514/6.2019-3527

Scale Adaptive Simulation of Stalled NACA 0012 Airfoil using high order schemes

Purvic Patel* and Yunchao Yang† and Gecheng Zha‡
Dept. of Mechanical and Aerospace Engineering
University of Miami, Coral Gables, Florida 33124
E-mail: gzha@miami.edu

A Scale Adaptive Simulation (SAS) is implemented with the Spalart-Allmaras (SA) turbulence model to evaluate its capability for flows with massive separation. A subsonic flat plate case is validated and the results are compared with SA and other hybrid turbulence models. The Mean Stress Depletion (MSD) problem, aroused in the case of the Detached-Eddy Simulation (DES97), is not observed with the SAS turbulence model under ambiguous grid. Subsequently, NACA 0012 airfoil is investigated for post-stall regime and predicted aerodynamics performance is compared with the experimental, URANS and IDDES results. The predicted lift and drag coefficients using the SAS and IDDES agree well with the experiment, significantly more accurate than the results of URANS. Apart from these quantitative results, the turbulent flow structures obtained with hybrid turbulence models reveal more details of the small structures.

I. Nomenclature

L_{ref}	=	Reference length
ρ_∞	=	Freestream density
U_∞	=	Freestream velocity
μ_∞	=	Freestream dynamics viscosity
Ω	=	Vorticity
Re	=	Reynolds number
$i,\ j,\ k$	=	Dummy indices for Indicial / Einstein summation notation
κ	=	von Karman constant
Δt	=	Physical time step
$\Delta\tau$	=	Pseudo time step
$U,\ V,\ W$	=	Contravariant velocities in ξ, η and ζ directions
P_ν	=	Production of turbulence viscosity
D_ν	=	Destruction of turbulence viscosity
T_ν	=	Trip term for turbulence viscosity
Δq	=	Difference between the velocity at the field point and that at the trip (on the wall)
Δx_t	=	Grid spacing along the wall at the trip
ω_t	=	Wall vorticity at the trip
d_t	=	Distance from the field point to the trip
δ	=	Boundary layer thickness
SA-noft2	=	Spalart-Allmaras One-Equation Model without f_{t2} Term
LES	=	Large Eddy Simulation
DES	=	Detached-Eddy Simulation
DDES	=	Delayed Detached-Eddy Simulation
IDDES	=	Improved Delayed Detached-Eddy Simulation
WMLES	=	Wall-Modeling in LES
SAS	=	Scale Adaptive Simulation

*Ph.D. Candidate
†Ph.D., AIAA member
‡Professor, ASME Fellow, AIAA associate Fellow.

II. Introduction

A flow separation is common in various industrial applications such as aviation, turbomachinery, automobile, etc. A flow separation affects the efficiency of a fluid machine and therefore its effects need to be understood so that the design can be optimized to mitigate its detrimental effects. In a case of massive flow separation, a flow field is enriched in physics involving shear layer instability, Kelvin-Helmholtz instability and large scale momentum carrying eddies. This enriched flow field is common for a post-stall regime of an airfoil which can occur during its pitching at a higher angle of attack or flight maneuvering under an extreme environment. This necessitates a turbulence model giving more insights into the flow physics and accurate quantitative aerodynamic performance of the stalled airfoil.

A Reynolds-Averaged Navier–Stokes (RANS) turbulence model performs better with a thin shear layer like an attached or a mildly separated flow. In this case, boundary layer thickness is small and the vortices are of the length scales much smaller than the geometry. With a massive flow separation, a flow field contains vortical structures and the length scale of large momentum carrying eddies is comparable to the geometry scale [1]. This is especially a problematic scenario for a RANS turbulence model as it models all turbulent spectrum eddies with the same length scale.

A Large Eddy Simulation (LES) relies on the notion that small scale eddies are more isotropic. This allows modeling their effects whereas the large, energy containing eddies are resolved to account for their effects on the momentum and energy equation. In the LES, the time-dependent Navier-Stokes equations (NS) are filtered in a physical space. Eddies smaller than the filter width are modeled and their effects on the filtered NS equations governing larger eddies are accounted by the Sub-Grid Scale (SGS) stress tensor. This make the LES more general and accurate than a RANS turbulence model as it carries more flow physics. This also entices its usage for a numerical simulation however resolving a boundary layer with a LES is computationally too expensive and still out of reach today for many high Reynolds number industrial applications [1, 2].

Hybrid RANS/ LES turbulence models are developed to take advantages of RANS for thin shear layer and LES for massively separated flows. In 1997, Spalart et al. [1] proposed the Detached Eddy Simulation (DES) based on one equation Spalart-Allmaras (SA) turbulence model. This model is commonly referred as DES97 in research community. This model is originally developed to use a RANS mode in the boundary layer and LES away from a wall. A switch from RANS to LES is designed based on a local grid size information. This explicit grid size dependence for different mode is found troublesome when a wall parallel grid spacing falls below the boundary layer thickness with a systematic mesh refinement. This creates premature transition to the LES mode within a boundary layer thickness with a reduction in eddy viscosity and thereby modeled Reynolds stress [3, 4]. However, this modeled Reynolds stress is reduced below the RANS level and the resolved Reynolds stresses arising from the LES is not strong enough to restore the modeled Reynolds stress of the RANS. This Modeled Stress Depletion (MSD) leads to the Grid Induced Separation [3].

To tackle this MSD problem, Spalart et al. [3] introduced a blending function, similar to the one used by Menter et al. [5], to shield the boundary layer and preserve the RANS mode in it and delay the LES mode. This newer version of DES is referred as Delayed Detached Eddy Simulation (DDES). However, based on Spalart et al. [3] DDES would also suffer from the MSD only in extreme grids. Use of DES97 for wall-modeling in LES (WMLES) by Nikitin el al. [6] for planar channel flow showed mismatch between modeled and resolved log layer, termed as Log Layer Mismatch (LLM). Later Shur et al. [7] proposed the Improved Delayed Detached Eddy Simulation (IDDES) aimed at wall modeling in the LES (WMLES) and it also addresses the LLM and MSD problem faced by the DES97, and DDES.

In an alternative approach to the DES, Menter et al. [8] developed the KE1E one-equation model for the eddy-viscosity, which is an improved URANS method providing the LES like behavior in detached flow regions. Here, the destruction term relies on the von Karman length scale [9] and not on a distance away from the wall. Introduction of this length scale allows model to adjust dynamically to the resolved stresses and provides the LES like behavior in separated flow regions without an explicit grid dependence. This concept is coined as Scale-Adaptive-Simulation [8]. Menter et al. [10] presented two equation turbulence model $k - \nu_t$ operating in the RANS and SAS mode. The same concept is extended later to the SST two equation turbulence model using ω as second length scale. Recently, this concept is extended to the SA turbulence model. Xu et al. [11] modified the distance term appearing in the destruction term whereas Coder [12] provided SAS capability to the original SA turbulence model by introducing an additional destruction term relying on the von Karman length scale.

In this paper, the SAS concept is extended to the SA turbulence model similar to the work of Xu et al. [11]. However, the strain rate is used as first order velocity gradient instead of vorticity to calculate the von Karman length scale. To validate its implementation, firstly a subsonic flat plate case is investigated using high order numerical schemes. Subsequently, post-stall simulations of NACA 0012 airfoil are carried out to validate its capability under a massive flow

separation. The results of these cases are presented in the code validation section.

III. Governing equations

The spatially filtered compressible Navier-Stokes equations along with one equation SA turbulence model are solved in fully coupled manner using an implicit unfactored Gauss-Seidel line iteration to achieve high convergence rate. These equations are nondimensionalized using L_{ref}, ρ_∞, U_∞ and μ_∞ and the governing equations in generalized coordinates are given by:

$$\frac{\partial Q}{\partial t} + \frac{\partial E}{\partial \xi} + \frac{\partial F}{\partial \eta} + \frac{\partial G}{\partial \zeta} = \frac{1}{Re}\left[\frac{\partial R}{\partial \xi} + \frac{\partial S}{\partial \eta} + \frac{\partial T}{\partial \zeta}\right] + S_v \tag{1}$$

where,

$$Q = \frac{1}{J}\begin{bmatrix}\rho\\ \rho u\\ \rho v\\ \rho w\\ \rho e\\ \rho\tilde{\nu}\end{bmatrix}, E = \begin{bmatrix}\rho U\\ \rho uU + pl_x\\ \rho vU + pl_y\\ \rho wU + pl_z\\ (\rho e + p)U - pl_t\\ \rho\tilde{\nu}U\end{bmatrix}, F = \begin{bmatrix}\rho V\\ \rho uV + pm_x\\ \rho vV + pm_y\\ \rho wV + pm_z\\ (\rho e + p)V - pm_t\\ \rho\tilde{\nu}V\end{bmatrix}$$

$$G = \begin{bmatrix}\rho W\\ \rho uW + pn_x\\ \rho vW + pn_y\\ \rho wW + pn_z\\ (\rho e + p)W - pn_t\\ \rho\tilde{\nu}W\end{bmatrix}, R = \begin{bmatrix}0\\ \tau_{xi}l_i\\ \tau_{yi}l_i\\ \tau_{zi}l_i\\ (u_j\tau_{ij} - q_i)l_i\\ \frac{\rho}{\sigma}(\nu + \tilde{\nu})\frac{\partial\tilde{\nu}}{\partial x_i}l_i\end{bmatrix}, S = \begin{bmatrix}0\\ \tau_{xi}m_i\\ \tau_{yi}m_i\\ \tau_{zi}m_i\\ (u_j\tau_{ij} - q_i)m_i\\ \frac{\rho}{\sigma}(\nu + \tilde{\nu})\frac{\partial\tilde{\nu}}{\partial x_i}m_i\end{bmatrix} \tag{2}$$

$$T = \begin{bmatrix}0\\ \tau_{xi}n_i\\ \tau_{yi}n_i\\ \tau_{zi}n_i\\ (u_j\tau_{ij} - q_i)n_i\\ \frac{\rho}{\sigma}(\nu + \tilde{\nu})\frac{\partial\tilde{\nu}}{\partial x_i}n_i\end{bmatrix}, S_v = \frac{1}{J}\begin{bmatrix}0\\ 0\\ 0\\ 0\\ 0\\ P_\nu - D_\nu + T_\nu + \frac{1}{Re}\frac{\rho}{\sigma}c_{b2}\frac{\partial\tilde{\nu}}{\partial x_i}\frac{\partial\tilde{\nu}}{\partial x_i}\end{bmatrix}$$

The conservative variable vector Q consists of density (ρ), cartesian velocity components ($u,\ v,\ w$) in ($x,\ y,\ z$) direction respectively multiplied by density, total internal energy (ρe), and modified turbulent viscosity ($\rho\tilde{\nu}$). The viscous term vectors R, S, and T are represented in indicial notations, using dummy indices i and j, in Eq. (2). S_v represents the SA turbulence model source term.

$$\begin{aligned} l &= \frac{\partial\xi_{,i}}{J},\ m = \frac{\partial\eta_{,i}}{J},\ n = \frac{\partial\zeta_{,i}}{J}\\ l_t &= \frac{\xi_t}{J},\ m_t = \frac{\eta_t}{J},\ n_t = \frac{\zeta_t}{J}\end{aligned} \tag{3}$$

$$\begin{aligned} U &= l_t + l_iV_i = l_t + l_xu + l_yv + l_zw\\ V &= m_t + m_iV_i = m_t + m_xu + m_yv + m_zw\\ W &= n_t + n_iV_i = n_t + n_xu + n_yv + n_zw\end{aligned} \tag{4}$$

where $l_t,\ m_t,\ n_t$ are the components of the interface contravariant velocity of the control volume in $\xi,\ \eta,\ \zeta$ directions respectively. $l,\ m,\ n$ represent the normal vectors with their magnitudes equal to the elemental surface areas and pointing to the direction of increasing $\xi,\ \eta,\ \zeta$, respectively. J is the Jacobian of the coordinate transformation. Contravariant variant velocities $U,\ V,\ W$ in $\xi,\ \eta,\ \zeta$ direction respectively are given by Eq. (4).

$$\rho e = \frac{p}{(\gamma-1)} + \frac{1}{2}\rho(u^2+v^2+w^2) \tag{5}$$

The total internal energy (ρe) and static pressure (p) are related by Eq. (5). The shear stress and total heat flux (q_i) are given by

$$\begin{aligned} \tau_{ij} &= \tau_{ij}^{lam} + \tau_{ij}^{turb} = \frac{1}{Re}\left[(\mu+\mu_t)\left(\frac{\partial u_i}{\partial x_j} + \frac{\partial u_j}{\partial x_i} - \frac{2}{3}\delta_{ij}\frac{\partial u_k}{\partial x_k}\right)\right] \\ q_i &= \frac{1}{M_\infty^2}\frac{1}{\gamma-1}\left(\frac{\mu}{Pr} + \frac{\mu_t}{Pr_t}\right)\frac{\partial T}{\partial x_i} \end{aligned} \tag{6}$$

where the turbulent viscosity (μ_t) is determined by the SA turbulence model. Molecular viscosity (μ) is calculated using Sutherland's law. The source term (S_ν) of the SA equation consists of production, destruction, trip and diffusion terms.

$$\begin{aligned} P_\nu &= \rho c_{b1}(1-f_{t2})\hat{S}\tilde{\nu} \\ D_\nu &= \frac{1}{Re}\left[\rho\left(c_{w1}f_w - \frac{c_{b1}}{\kappa^2}f_{t2}\right)\left(\frac{\tilde{\nu}}{d_w}\right)^2\right] \\ T_\nu &= Re\left[\rho f_{t1}(\Delta q)^2\right] \end{aligned} \tag{7}$$

where P_ν, D_ν and T_ν are the production, destruction and trip terms, respectively and their values are calculated using relations given in Eq. (8).

$$\begin{aligned} &\mu_t = \rho\tilde{\nu}f_{v1}\,, && \chi = \frac{\tilde{\nu}}{\nu}\,, && f_{v1} = \frac{\chi^3}{\chi^3+c_{v1}^3} \\ &\hat{S} = \Omega + \overline{S}\,, && f_{v2} = 1 - \frac{\chi}{1+\chi f_{v1}}\,, && f_w = g\left(\frac{1+c_{w3}^6}{g^6+c_{w3}^6}\right)^{1/6} \\ &g = r + c_{w2}(r^6 - r)\,, && r = min\left(\frac{\tilde{\nu}}{\hat{S}\kappa^2 d_w^2}, 10\right)\,, && f_{t2} = c_{t3}\exp\left(-c_{t4}\chi^2\right) \\ &f_{t1} = c_{t1}g_t\exp\left[-c_{t2}\frac{\omega_t^2}{\Delta U^2}\left(d_w^2 + g_t^2 d_t^2\right)\right]\,, && g_t = min\left(0.1, \frac{\Delta q}{\omega_t \Delta x_t}\right)\,, && \overline{S} = \frac{1}{Re}\frac{\tilde{\nu}}{\kappa^2 d_w^2}f_{v2} \end{aligned} \tag{8}$$

Constants used in Eqs. (2), (7) and (8) are:

$$\begin{aligned} &c_{b1} = 0.1355\,, && \sigma = \frac{2}{3}\,, && c_{b2} = 0.622\,, && \kappa = 0.41 \\ &c_{w2} = 0.3\,, && c_{w3} = 2\,, && c_{v1} = 7.1\,, && c_{t3} = 1.1 \\ &c_{t4} = 2.0\,, && c_{w1} = \frac{c_{b1}}{\kappa^2} + \frac{(1+c_{b2})}{\sigma}\,, && c_{t1} = 1.0\,, && c_{t2} = 2.0 \end{aligned} \tag{9}$$

As most of the time the SA turbulence model is used for fully turbulent flow, trip term T_ν and f_{t2} are considered zero similar to SA-noft2 turbulence model and all the simulations in this study are carried out using SA-noft2 form of turbulence model.

A. Modification for SA turbulence model

In order to avoid numerical difficulties arising from zero or negative $\hat{S}$, the modification, as in Eq. (11), is applied in the present study to the P_ν of SA turbulence model source term.

$$\overline{S} = \frac{1}{Re}\frac{\tilde{\nu}}{\kappa^2 d_w^2}f_{v2} \tag{10}$$

$$\hat{S} = \begin{cases} \Omega + \overline{S} & : \overline{S} \geq -c_2\Omega \\ \Omega + \frac{\Omega(c_2^2\Omega + c_3\overline{S})}{(c_3-2c_2)\Omega - \overline{S}} & : \overline{S} < -c_2\Omega \end{cases} \tag{11}$$

where, $c_2 = 0.7$, $c_3 = 0.9$ and set $r = 10$ if $\hat{S} = 0$.

B. Distance scale modification for SA-DES turbulence model [1]

In the case of SA-DES, a turbulence model works in RANS mode close to the wall and in LES mode in detached boundary layer region. This behavior is achieved by replacing the distance scale d_w in the SA turbulence model by:

$$\tilde{d} = \min\left(d_w, C_{DES}\Delta_{max}\right) \tag{12}$$

where, $C_{DES} = 0.65$ is a constant and $\Delta_{max} = \max\left(\Delta_x, \Delta_y, \Delta_z\right)$

It can be seen from Eq. (12) that the distance scale depends explicitly on the local grid size away from the wall to achieve LES behavior.

A refinement of mesh and time is the foundation of CFD to validate the convergence of a result. Therefore, a systematic mesh refinement with the DES should offer converged results however many researchers have observed grid induced separation [3, 5]. The reason for this behavior is attributed to an abrupt switch to LES without providing enough modeled Reynolds stress and this Modeled Stress Depletion (MSD) gives rise to the flow separation. To overcome this MSD problem, Spalart et al. developed the DDES turbulence model and later Shur et al. proposed the IDDES turbulence model which combines the advantage of DDES and WMLES.

C. Distance scale modification for SA-IDDES turbulence model [7]

The IDDES includes two branches, DDES and WMLES, and a set of empirical functions designed to obtain correct performance from these branches themselves. These models are coupled ensuring a favorable response of the combined model as DDES or WMLES depending on the inflow (or initial) conditions used in the simulation [7]. Here, d_w appearing in the SA turbulence model is replaced by l_{IDDES}, which is obtained by blending two different distance scales.

$$l_{IDDES} = \tilde{f}_d(1 + f_e)l_{RANS} + (1 - \tilde{f}_d)l_{LES} \tag{13}$$

In Eq. (13), l_{RANS} refers to the d_w of the SA model and l_{LES} is the length scale of LES model. l_{LES} length scale is defined via the subgrid length scale (Δ) as

$$\begin{aligned} l_{LES} &= C_{DES}\Psi\Delta \\ \text{where, } \Delta &= \min\{\max[C_w d_w, C_w\Delta_{max}, h_{wn}], \Delta_{max}\} \end{aligned} \tag{14}$$

h_{wn} in Eq. (14) represents the grid step in the wall-normal direction and empirical constant $C_w = 0.15$. In a case of multi-block parallel simulation with the wall in multiple directions, finding h_{wn} is difficult as it needs wall normal minimum distance direction information.

Blending function $\tilde{f}_d$ and experimental function f_e used in the model are given by:

$$\begin{aligned} \tilde{f}_d &= \max\left(1 - f_{dt}\ ,\ f_B\right) \\ f_e &= \max\left[(f_{e1} - 1), 0\right]\Psi f_{e2} \end{aligned} \tag{15}$$

where, f_{dt}, f_B, Ψ, f_{e2} and f_{e1} are

$$\begin{aligned} f_{dt} &= 1 - \tanh[(8r_{dt})^3] \\ f_B &= \min\left\{2\exp\left(-9\alpha^2\right), 1.0\right\} \text{ with } \alpha = 0.25 - (d_w/\Delta_{max}) \\ \Psi^2 &= \min\left[10^2, \frac{1 - \frac{c_{b1}}{c_{w1}\kappa^2 f_w^*}[f_{t2} + (1 - f_{t2})f_{v2}]}{f_{v1}\max(10^{-10}, 1 - f_{t2})}\right] \text{ with } f_w^* = 0.424 \\ f_{e2} &= 1.0 - \max\left(f_t, f_l\right) \\ f_{e1}\left(d_w/\Delta_{max}\right) &= \begin{cases} 2\exp\left(-11.09\alpha^2\right) & : \alpha \geq 0 \\ 2\exp\left(-9.0\alpha^2\right) & : \alpha \leq 0 \end{cases} \end{aligned} \tag{16}$$

Here, f_{e2} depends on f_t and f_l, which are given by

$$\begin{aligned} f_t &= \tanh\left[(c_t^2 r_{dt})^3\right] \text{ with } r_{dt} = \frac{\nu_t}{\max\left(\sqrt{u_{i,j}u_{i,j}}\,,\,10^{-10}\right)\kappa^2 d_w^2 Re} \\ f_l &= \tanh\left[(c_l^2 r_{dl})^{10}\right] \text{ with } r_{dl} = \frac{\nu}{\max\left(\sqrt{u_{i,j}u_{i,j}}\,,\,10^{-10}\right)\kappa^2 d_w^2 Re} \end{aligned} \tag{17}$$

Δ_{max} appearing in Eq. (16) is similar to the one used in DES.

D. Distance scale modification for SA-SAS turbulence model

A length scale (L_{vk}) is similar to the mixing length based on von Karman's similarity hypothesis, where the mixing length depends on the velocity distribution instead of its magnitude [13].

$$L_{vk} = \kappa \left| \frac{S}{\sqrt{\frac{\partial^2 u_i}{\partial x_j \partial x_j}\frac{\partial^2 u_i}{\partial x_m \partial x_m}}} \right| \tag{18}$$

$$d_w = \min\left(d_w\,,\,\max\left(\frac{L_{vk}}{\kappa}\,,\,C_{des}\Delta_{max}\right)\right) \tag{19}$$

This length scale allows model to adjust dynamically under massive flow separation. The DES limiter is introduced in its length scale to avoid singularity arising from $1/L_{vk}$ under mean-strain rate approaching to zero. This limiter also allows high wave number damping to dissipate energy to the smallest scale rather than accumulating. With the presence of sufficiently strong instability or initially resolved flow, this model allows the formation of a turbulent spectrum [14]. In a Kolmogorov spectrum, the smallest scales dominate first and second order velocity derivatives, thereby L_{vk} adjusts to the smallest scales to allow the formation of the turbulent spectrum[14]. Xu et al. [11] used vorticity as first order velocity gradient instead of strain rate to evaluate the length scale.

IV. Time marching scheme

Introducing fictitious time (τ) [15] in Eq. (1), the governing equations can be re-written as Eq. (20). A second order backward difference scheme with three stencil used for $\frac{\partial Q}{\partial t}$ is given by Eq. (21). In each physical time step (Δt), the solution is advanced by fictitious time step ($\Delta\tau$) using local time stepping in order to reduce residual $\mathcal{R}^*$ to zero. A pseudo time step is discretized using first-order Euler scheme.

$$\frac{\partial Q}{\partial \tau} = \mathcal{R}(Q^{n+1}) - \frac{\partial Q}{\partial t} = \mathcal{R}^*(Q^{n+1}) \tag{20}$$

$$\frac{\partial Q}{\partial t} = \frac{3Q^{n+1} - 4Q^n + Q^{n-1}}{2\Delta t} \tag{21}$$

where $n+1,\ n,\ n-1$ are three sequential time steps.

Final form of semi-discretized governing equations are given by:

$$\left[\left(\frac{1}{\Delta\tau} + \frac{1.5}{\Delta t}\right) I - \left(\frac{\partial \mathcal{R}}{\partial Q}\right)^{n+1,m}\right] \delta Q^{n+1,m+1} = \mathcal{R}^{n+1,m} - \frac{3Q^{n+1,m} - 4Q^{n,m} + Q^{n-1,m}}{2\Delta t} \tag{22}$$

where $m,\ m+1$ are two consecutive pseudo time steps. $\mathcal{R}$ represents the net flux determined by the spatial dicretization of inviscid and viscous flux.

V. Numerical methods

In the present study, the Roe scheme [16, 17] is used for the inviscid flux evaluation. The conservative variables at the interface are reconstructed using 5^{th} order WENO scheme and 4^{th} order central differencing scheme is used for the viscous flux calculation.

A. 5th Order WENO Scheme [18–21]

For the inviscid flux evaluation, the conservative variables $Q_L,\ Q_R$ are reconstructed at the interface using 5^{th} order WENO scheme given by:

$$(Q_L)_{i+1/2} = \omega_0 q_0 + \omega_1 q_1 + \omega_2 q_2 \tag{23}$$

where,

$$\begin{aligned} q_0 &= \frac{1}{3}Q_{i-2} - \frac{7}{6}Q_{i-1} + \frac{11}{6}Q_i \\ q_1 &= -\frac{1}{6}Q_{i-1} + \frac{5}{6}Q_i + \frac{1}{3}Q_{i+1} \\ q_0 &= \frac{1}{3}Q_i - \frac{5}{6}Q_{i+1} - \frac{1}{6}Q_{i+2} \end{aligned} \tag{24}$$

$$\omega_k = \frac{\alpha_k}{\alpha_0 + \ldots + \alpha_{r-1}} \tag{25}$$

$$\begin{aligned} \alpha_k &= \frac{C_k}{\epsilon + IS_k}, k = 0, \ldots, r-1 \\ C_0 &= 1.1, C_1 = 0.6, C_2 = 0.3 \\ IS_0 &= \frac{13}{12}\left(Q_{i-2} - 2Q_{i-1} + Q_i\right)^2 + \frac{1}{4}\left(Q_{i-2} - 4Q_{i-1} + 3Q_i\right)^2 \\ IS_1 &= \frac{13}{12}\left(Q_{i-1} - 2Q_i + Q_{i+1}\right)^2 + \frac{1}{4}\left(Q_{i-1} - Q_{i+1}\right)^2 \\ IS_3 &= \frac{13}{12}\left(Q_i - 2Q_{i+1} + Q_{i+2}\right)^2 + \frac{1}{4}\left(Q_i - 4Q_{i+1} + Q_{i+2}\right)^2 \end{aligned} \tag{26}$$

where, IS_k are the smoothness operators and ϵ is a constant to safeguard against denominator becoming zero. In general, very small number for ϵ should be used, however Shen et al. [22] recommended $\epsilon = 10^{-2}$. Rationale behind this value has to do with the oscillation in the weights of WENO scheme which impairs the convergence rate as well as level. In this paper, $\epsilon = 10^{-2}$ is used even though flow field is shock free.

VI. Boundary conditions

At the inlet, stagnation quantities (i.e. total pressure and total temperature) and flow angles are defined. In the spanwise direction, a periodic boundary condition is used. A static pressure is defined at the outlet. Near the wall, no-slip wall boundary condition is employed with $\tilde{\nu} = 0$ and zero wall normal velocity in the inviscid flux, Eq. (2), is enforced.

VII. Code validation

Implementation of SAS turbulence model is validated with two different cases, namely flat plate and NACA 0012 airfoil. A subsonic flat plate case is used to study the effect of grid refinement on the predicted distributions in the boundary layer and thereby MSD problem under completely attached flow. To investigate further its capabilities under massive flow separation, NACA 0012 airfoil case is used at various angle of attacks beyond stall.

A. Flat plate

A subsonic flat plate is a classical test case used in research community to validate a turbulence model implementation. It is also used to investigate the grid sensitivity effect on the velocity profile with a hybrid turbulence model. The MSD problem is reported by many researchers with the DES turbulence model with an ambiguous grid density. Fig. 1 shows such an ambiguous grid used in the present study to validate the SAS turbulence model.

For the numerical simulation, Mach number 0.6 and 1.615×10^7 Reynolds number based on a flat plate length are used. A grid spacing of $\Delta_x = 1.5\delta_L$ is used near the inlet. At $Re_x = 1.2 \times 10^7$, $\Delta_x = 0.79\delta_L$ and ambiguous grid starts from this location based on the local boundary layer thickness. The computational grid is refined further progressively so that $\Delta_x = 0.026\delta_L$ near the outlet. In the spanwise direction, $\Delta_z = 0.1\delta_L$ is used. A grid spacing ensuring y^+ below 1 is used near the wall.

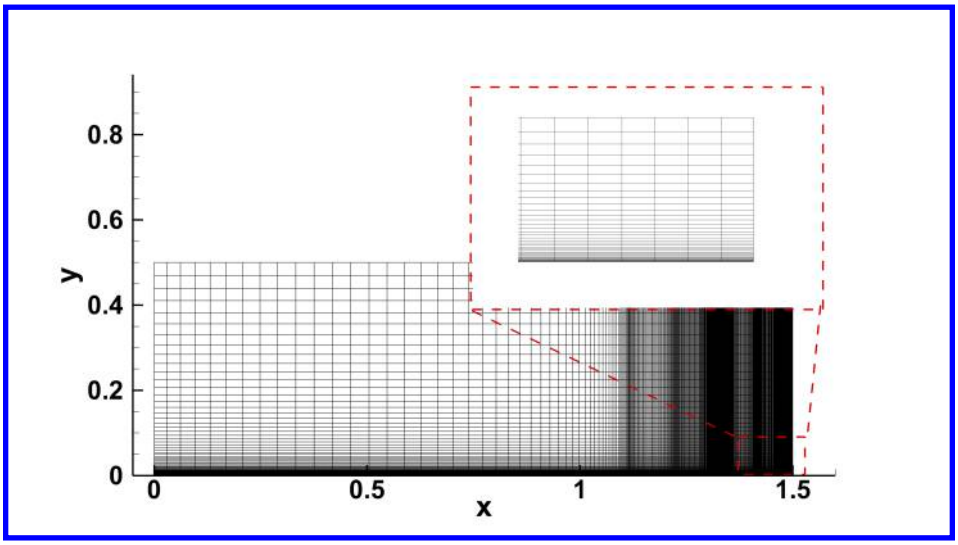

Fig. 1 Mesh overview

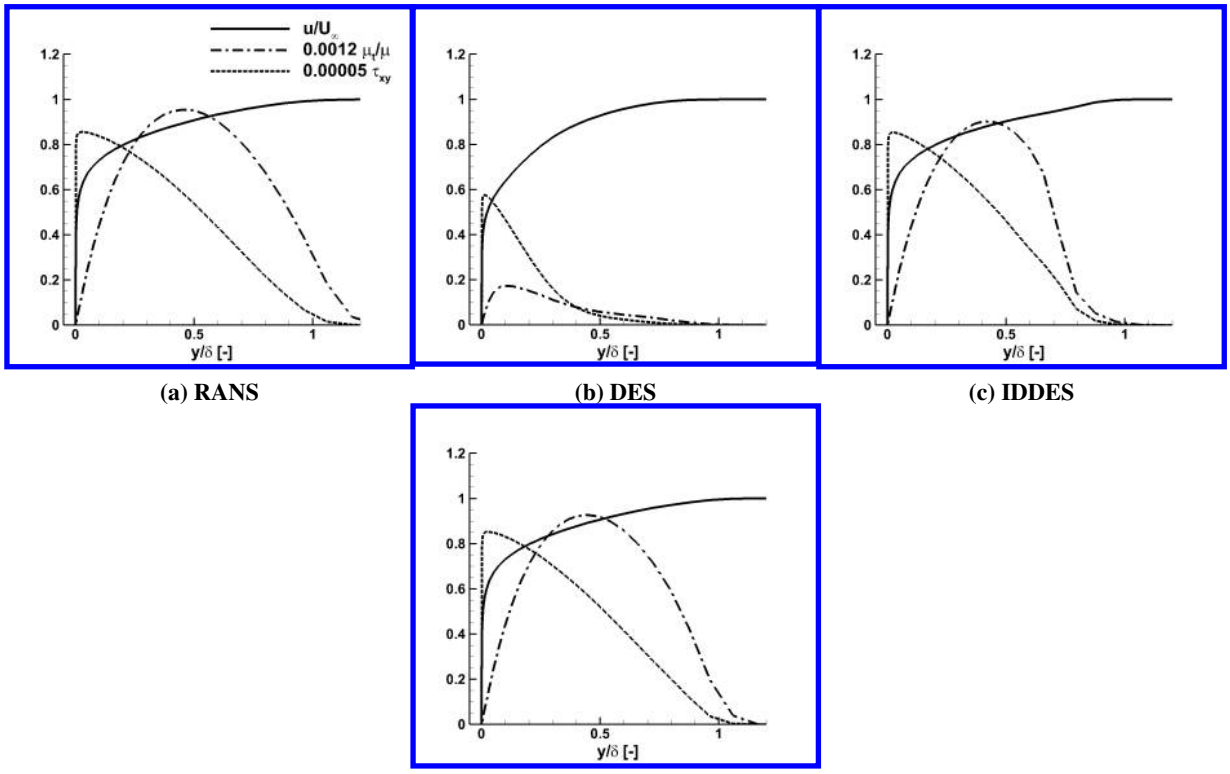

(a) RANS **(b) DES** **(c) IDDES**

(d) SAS

Fig. 2 Distributions in flat plate boundary layer, $Re_L = 1.615 \times 10^7$ and $\Delta_{\|} = 0.1\delta_L$

A distribution of streamwise velocity, turbulent viscosity and Reynolds shear stress (τ_{xy}) in the boundary layer is compared for the RANS, DES, IDDES and SAS turbulence models in Fig. 2. The τ_{xy} is calculated based on the normalized velocity and turbulent viscosity. These profiles are extracted at the outlet boundary. The MSD problem with the current ambiguous grid is clearly visible with the DES turbulence model in Fig. 2(b). It can be seen that the peak turbulent viscosity with the DES is only about 19 % of the RANS turbulence model and also the location of peak is quite different. The reason for this low turbulent viscosity is related to the LES mode in the boundary layer without providing enough resolved Reynolds stress. Similar MSD problem with an ambiguous grid is observed by Spalart et al. [3] and resulted in the development of a hybrid turbulence model addressing this issue. In the case of IDDES turbulence model, the turbulent viscosity is preserved fully with a sharp drop in it near the outer edge of boundary layer, similar to the DDES turbulence model [3]. Based on Spalart et al. [3], this deficit in the turbulent viscosity is very acceptable. With the SAS turulence model, the turbulent viscosity profile is also fully preserved and it follows more closely to the RANS model in comparison to the other hybrid turbulence models used in the present study. The turbulent stress profile with the IDDES and SAS are closely comparable to the RANS turbulence model.

B. NACA 0012 airfoil

Shur et al. [23] investigated the post-stall regime of NACA 0012 airfoil using DES and validated with the experimental results. This challenging massive flow separation case at higher angle of attack is used in the present study to investigate the application of SAS turbulence model. Further IDDES and URANS turbulence models are used to compare the predicted results with the measured lift and drag coefficients in the experiment.

For numerical simulations at different angle of attacks, the far-field is located at about 80 times airfoil chord length and in the spanwise direction, one chord length is used. O-mesh topology is used around the airfoil as it ensures high orthogonal grid near the wall. Grid refinement study is carried out to examine its effect on the quantitative and qualitative results of hybrid turbulence models. An overview of the different grid size is given in the Table 1. This grid size represents the number of nodes around the airfoil, in the direction normal to the wall and in the spanwise direction, respectively.

For an angle of attack study, the same computational grid is used. In the present study, Mach number of 0.5 and 1.3×10^6 Reynolds number based on one chord length are used. For the unsteady simulations, non-dimensional physical time step of 0.02 is used. Starting from the uniform flow field, the unsteady simulation is performed over 480 non-dimensional physical time with a pseudo CFL number of 3. In each physical time step, residuals are allowed to drop by three to four orders of magnitude, which is usually achieved within 15 pseudo time steps. For the predicted statistical time averaged lift and drag, initial 200 dimensionless time results are discarded to avoid initial flow transition effect.

Table 1 Computational grid for the NACA 0012 airfoil

Grid	Size	Δx	Δy	Δz	Δx^+	Δy^+	Δz^+
Coarse	192 x 100 x 30	0.00020–0.02681	1×10^{-5}	0.0344	10–1340	1	1720
Fine	288 x 100 x 30	0.00013–0.01788	1×10^{-5}	0.0344	6.6–894	1	1720

With mesh refinement at AoA= 45°, the predicted lift and drag coefficients are shown in Figs. 3 and 5. The statistical time averaged lift and drag coefficients are compared in Figs. 4 and 6. Similar study is carried out at AoA= 60° with predicted lift and drag coefficients, Figs. 7 and 9, and their statistical time averaged values, Figs. 8 and 10. A phase-locked vortex shedding with URANS can be seen in the predicted C_l and C_d over a time at both angle of attack which is usually not observed with massive flow separation in reality. IDDES and SAS show more realistic vortex shedding and chaotic turbulent flow structure with massive flow separation.

The statistical time averaged lift and drag coefficients, obtained by averaging between 200 to 480 dimensionless time, are given in Table 2 along with their experimentally measured values. Based on the fine mesh results, it is found that the RANS turbulence model over-predicts lift coefficient approximately 33 % and 28 % at 45° and 60° AoA, respectively. Similarly, it over-predicts drag coefficient approximately 24 % at both AoA. In the case of hybrid turbulence models with the fine mesh, the predicted lift and drag coefficients are in good agreement with the experiment except for the lift coefficient at 45° AoA.

Fig. 11 shows time-averaged isentropic Mach number distribution over an airfoil surface with different AoAs and meshes. It can be seen that the static pressure gradient in a streamwise direction remains same over suction surface

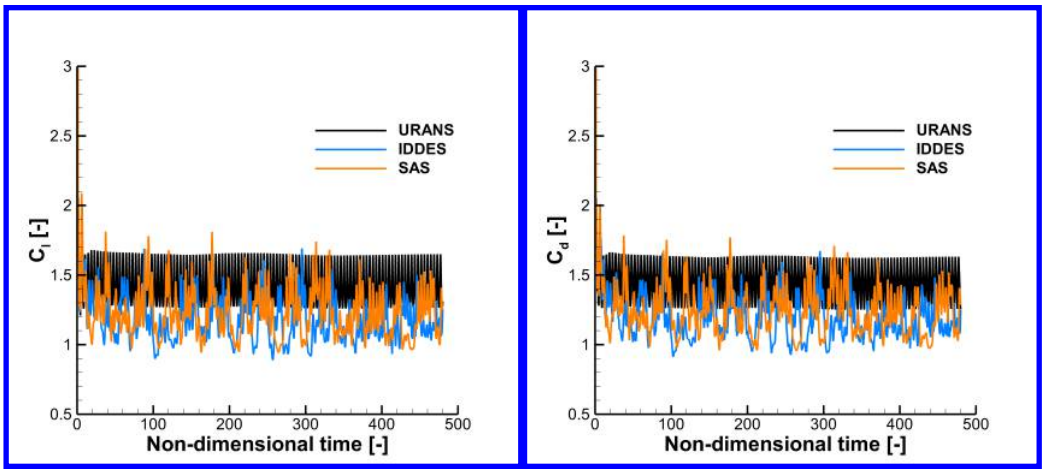

(a) C_l **(b)** C_d

Fig. 3 Variation in C_l and C_d at AoA= 45° with coarse mesh

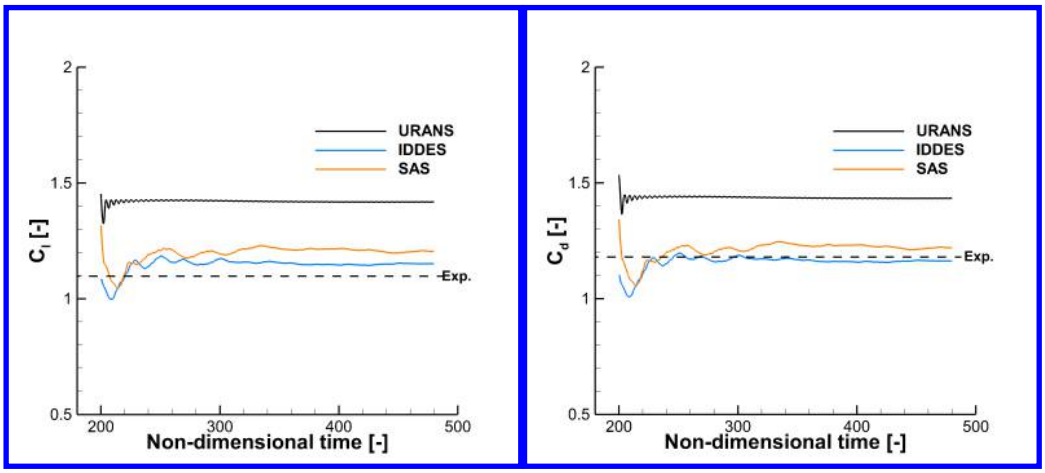

(a) C_l **(b)** C_d

Fig. 4 Time-averaged C_l and C_d at AoA= 45° with coarse mesh

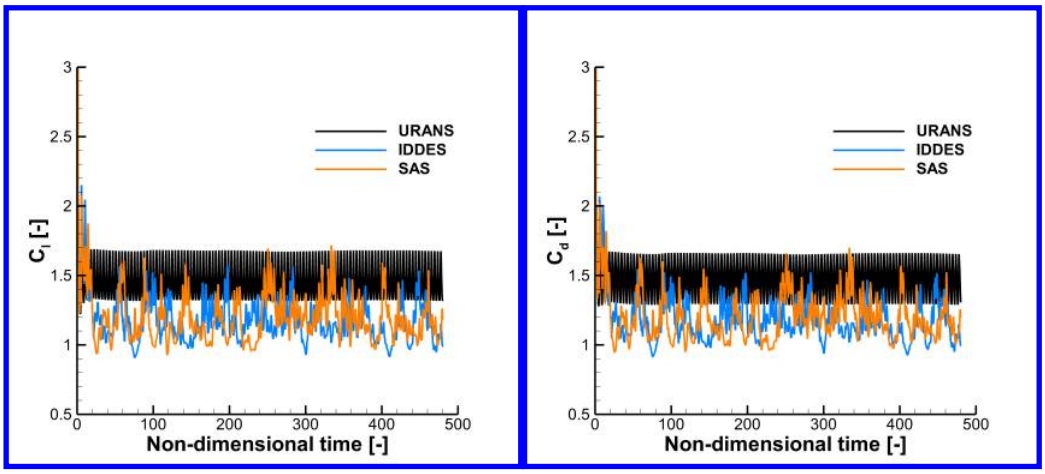

(a) C_l **(b)** C_d

Fig. 5 Variation in C_l and C_d at AoA= 45° with fine mesh

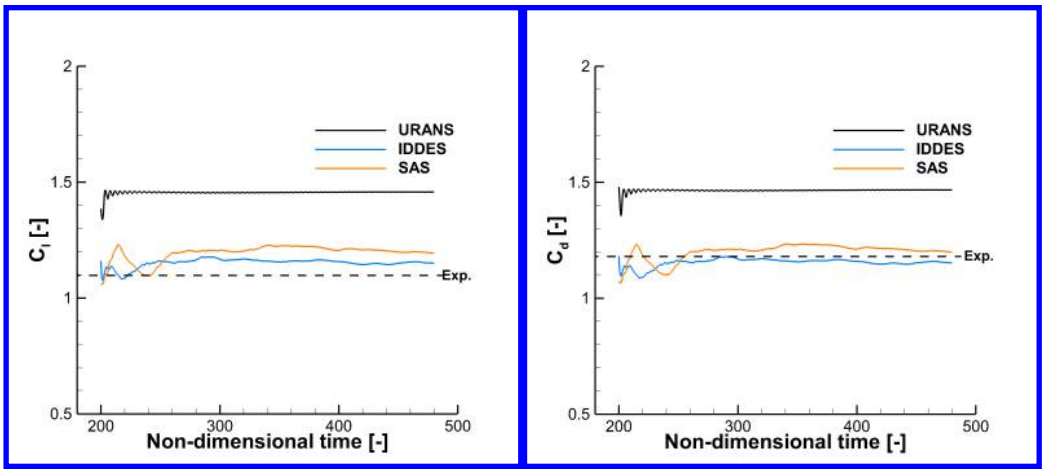

(a) C_l **(b)** C_d

Fig. 6 Time-averaged C_l and C_d at AoA= 45° with fine mesh

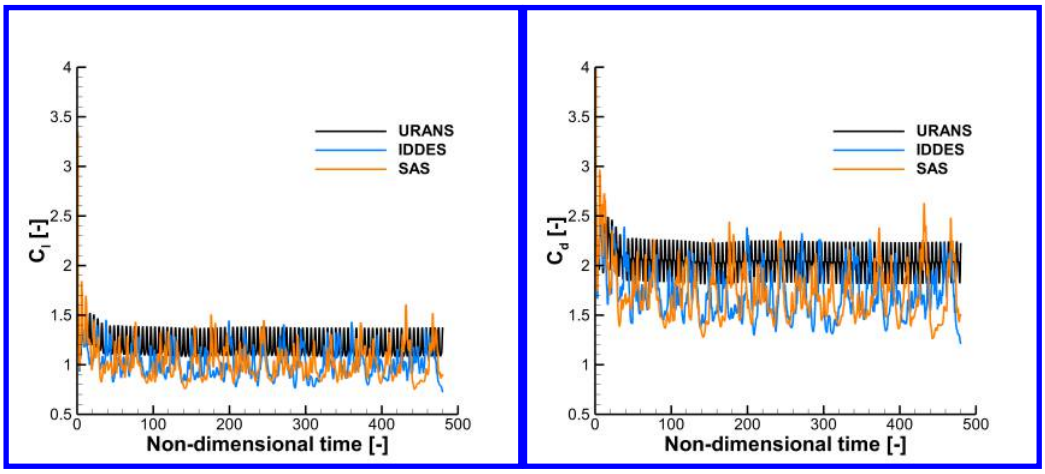

(a) C_l **(b)** C_d

Fig. 7 Variation in C_l and C_d at AoA= 60° with coarse mesh

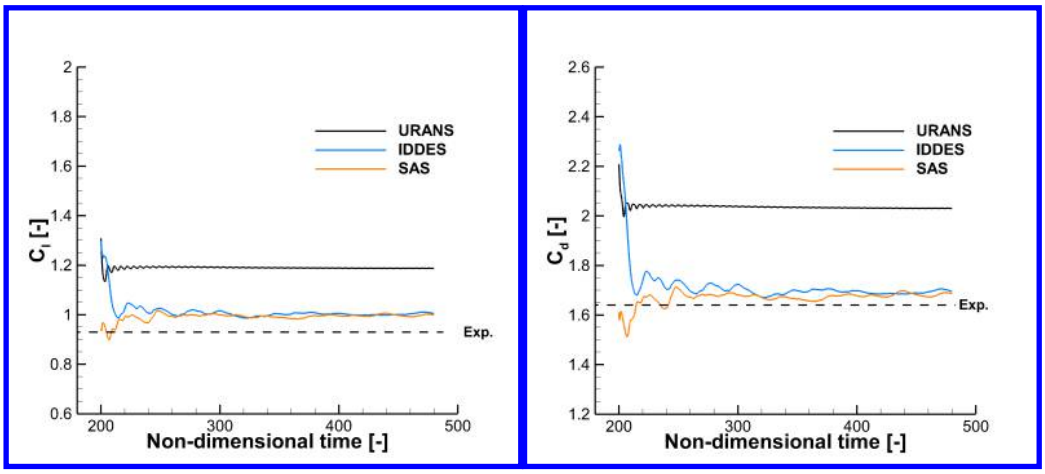

(a) C_l **(b)** C_d

Fig. 8 Time-averaged C_l and C_d at AoA= 60° with coarse mesh

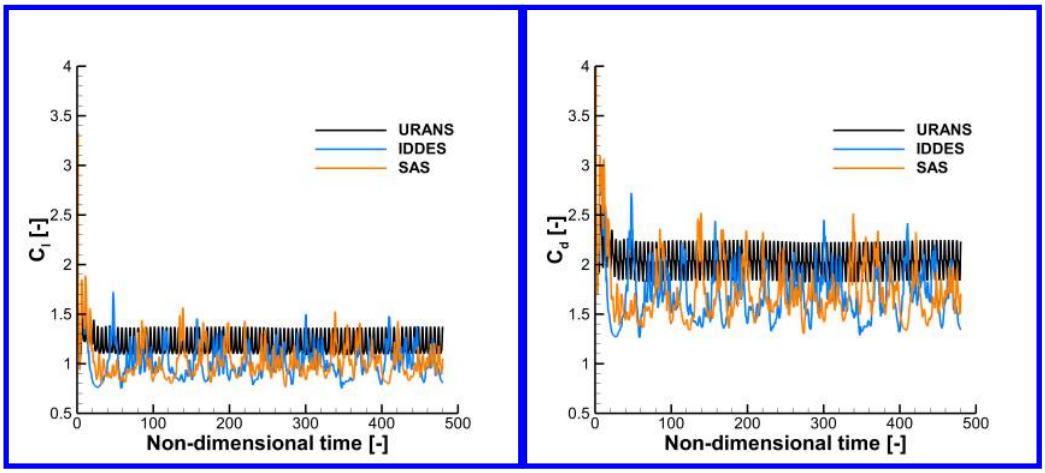

(a) C_l **(b)** C_d

Fig. 9 Variation in C_l and C_d at AoA= 60° with fine mesh

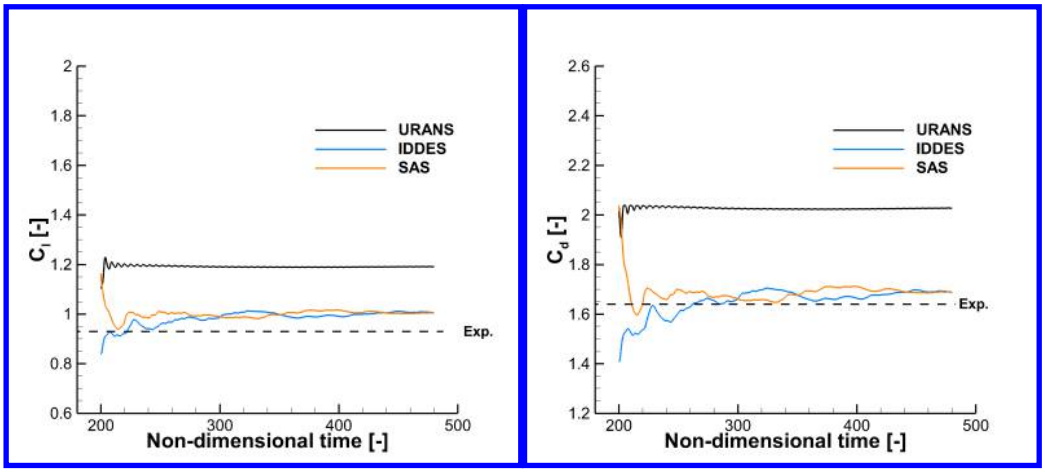

(a) C_l **(b)** C_d

Fig. 10 Time-averaged C_l and C_d at AoA= 60° with fine mesh

Table 2 C_l and C_d comparison

AoA	Turbulence model	C_l		C_d	
		Coarse	Fine	Coarse	Fine
45°	Experimental [23]	1.097		1.180	
	URANS	1.418	1.457	1.433	1.467
	IDDES	1.151	1.149	1.163	1.152
	SAS	1.205	1.194	1.220	1.200
60°	Experimental [23]	0.930		1.640	
	URANS	1.187	1.192	2.030	2.027
	IDDES	1.005	1.005	1.695	1.687
	SAS	1.000	1.004	1.687	1.689

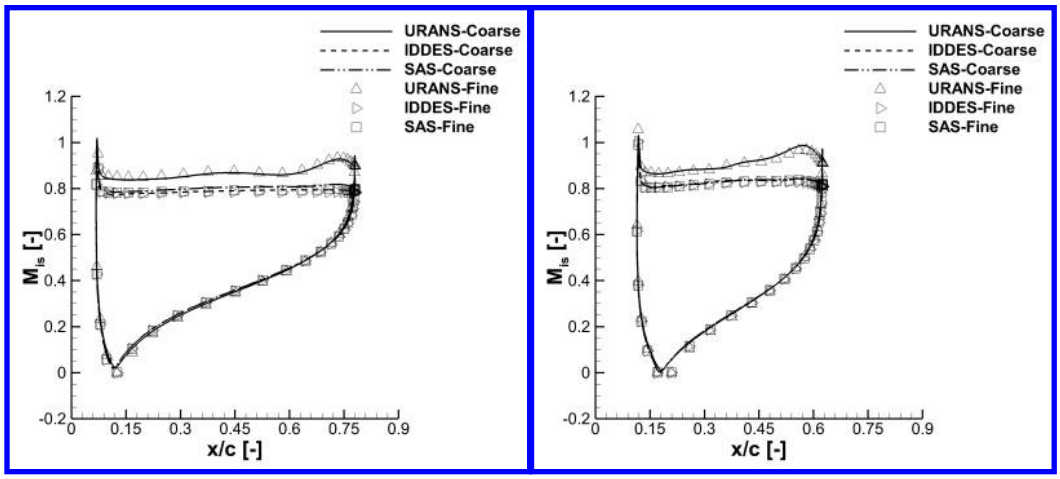

(a) At AoA= 45° **(b) At AoA**= 60°

Fig. 11 Time-averaged isentropic Mach number distribution of 50 % **span**

with all turbulence model except near trailing edge with the URANS. The URANS has consistently under-predicted static pressure in the massive flow separation region of airfoil suction surface which leads to the higher isentropic Mach number. As the area enclosed by the isentropic Mach profile is higher with the URANS, it predicts higher lift coefficient which is consistent with the values mentioned in Table 2. All turbulence models predict nearly the same static pressure over the pressure surface of airfoil except near leading and trailing edge of airfoil. On the pressure side, flow remains attached. This also shows that URANS and hybrid turbulence model behave similar in the attached flow region in the present study.

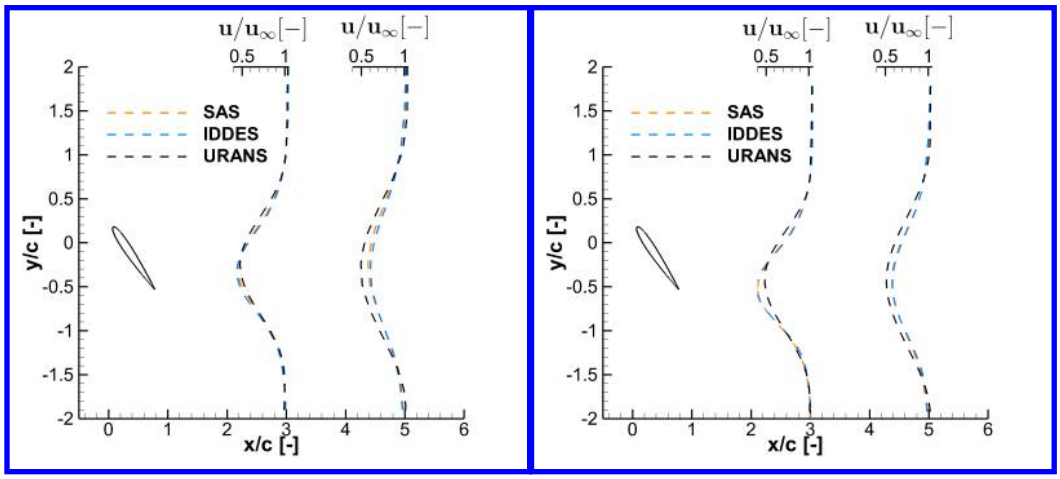

(a) Coarse mesh **(b) Fine mesh**

Fig. 12 Time-averaged wake profile of 50 % **span at AoA**= 45°

Time-averaged wake profile obtained with numerical simulations at different AoAs with mesh refinement is compared in Figs. 12 and 13. This wake profile is measured over a line. Its location, i.e. downstream from a leading edge, can be seen from the bottom abscissa and length of a probe line can be seen from the ordinate. A normalized streamwise velocity magnitude is shown in the top abscissa. It can be seen that the streamwise velocity with the URANS lags behind the hybrid turbulence models. This shows higher momentum deficit predicted by the URANS in a wake region behind the highly separated flow of an airfoil. Similar to the lift coefficient, this also shows a reason for the high drag coefficient with the URANS as compared to the hybrid turbulence models used in present study. With an increase in AoA, the wake becomes more stronger and thereby increases drag, Table 2.

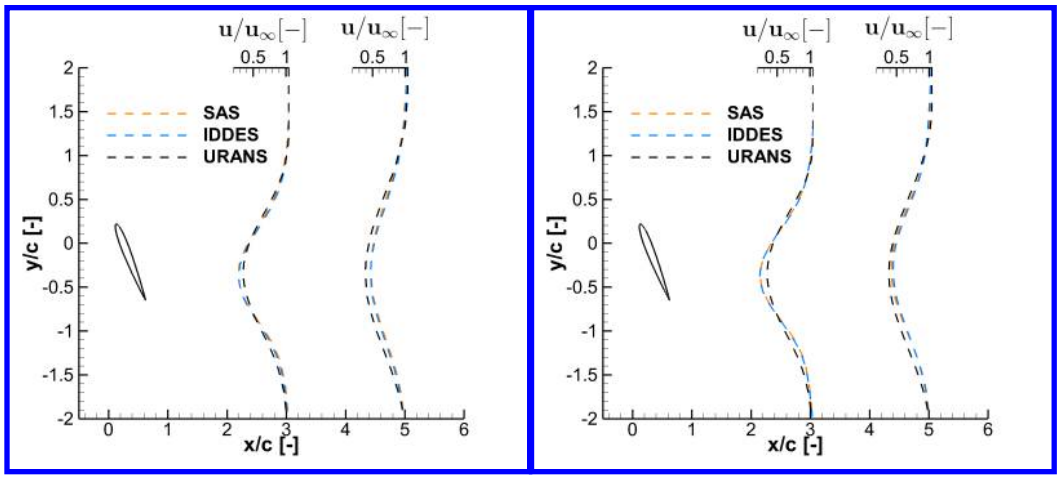

(a) Coarse mesh **(b) Fine mesh**

Fig. 13 Time-averaged wake profile of 50 % **span at AoA**= 60°

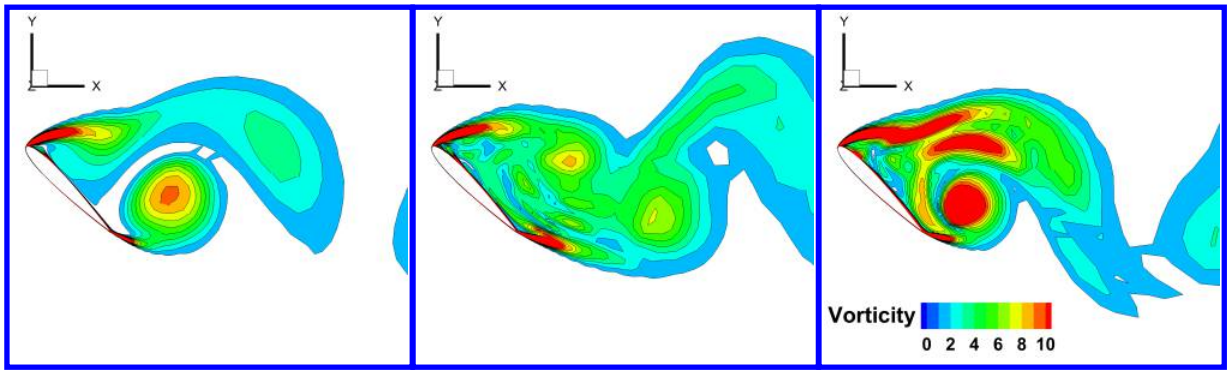

(a) URANS **(b) IDDES** **(c) SAS**

Fig. 14 Instantaneous vorticity of 50 % **span at AoA**= 45° **with coarse mesh**

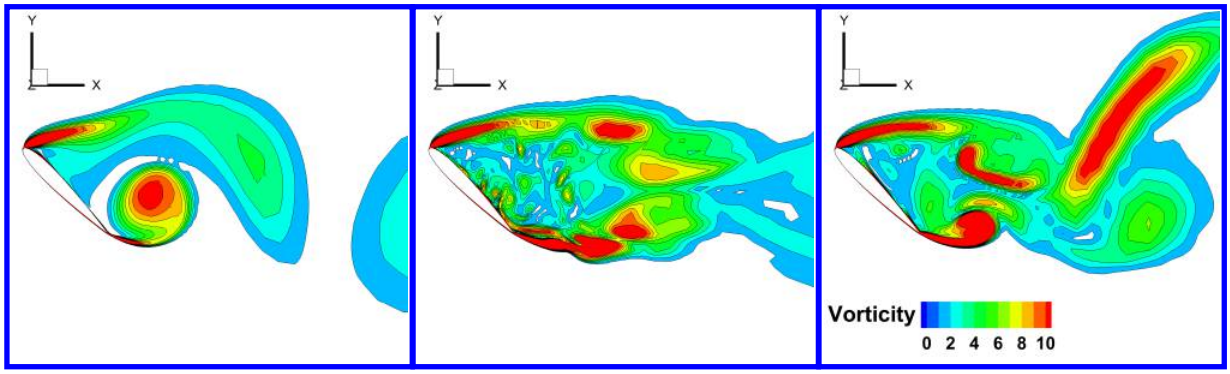

(a) URANS **(b) IDDES** **(c) SAS**

Fig. 15 Instantaneous vorticity of 50 % **span at AoA**= 45° **with fine mesh**

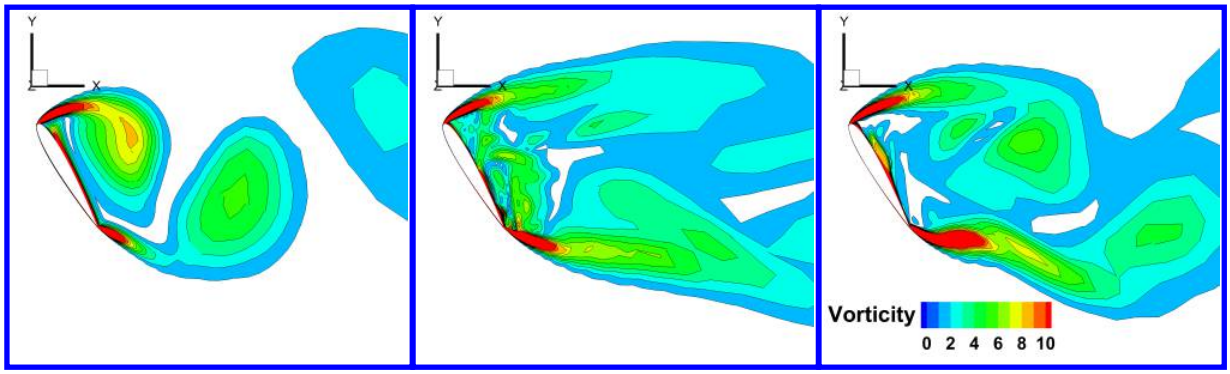

(a) URANS (b) IDDES (c) SAS

Fig. 16 Instantaneous vorticity of 50 % span at AoA= 60° with coarse mesh

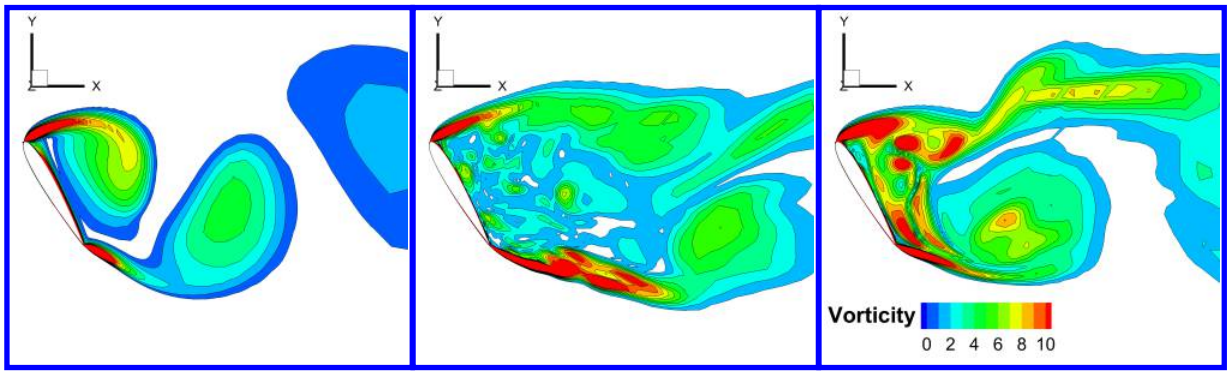

(a) URANS (b) IDDES (c) SAS

Fig. 17 Instantaneous vorticity of 50 % span at AoA= 60° with fine mesh

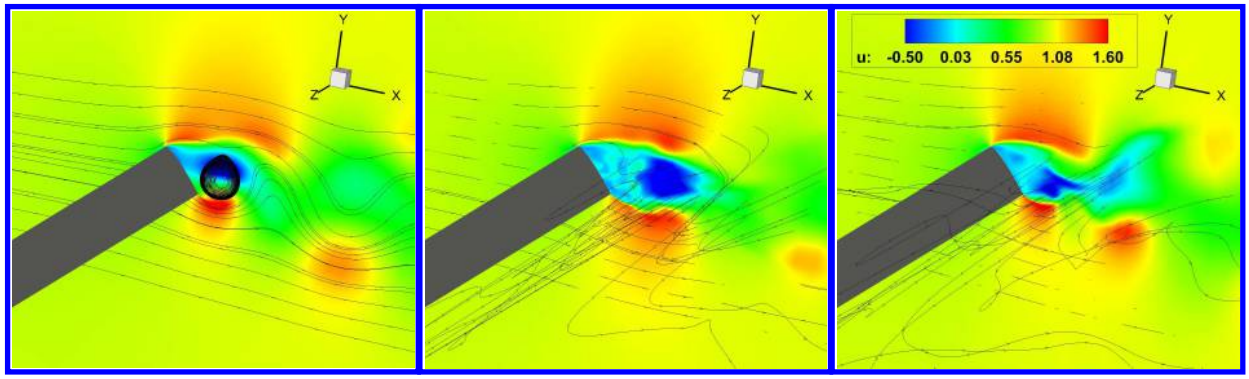

(a) URANS (b) IDDES (c) SAS

Fig. 18 Instantaneous streamlines at AoA= 45° with fine mesh

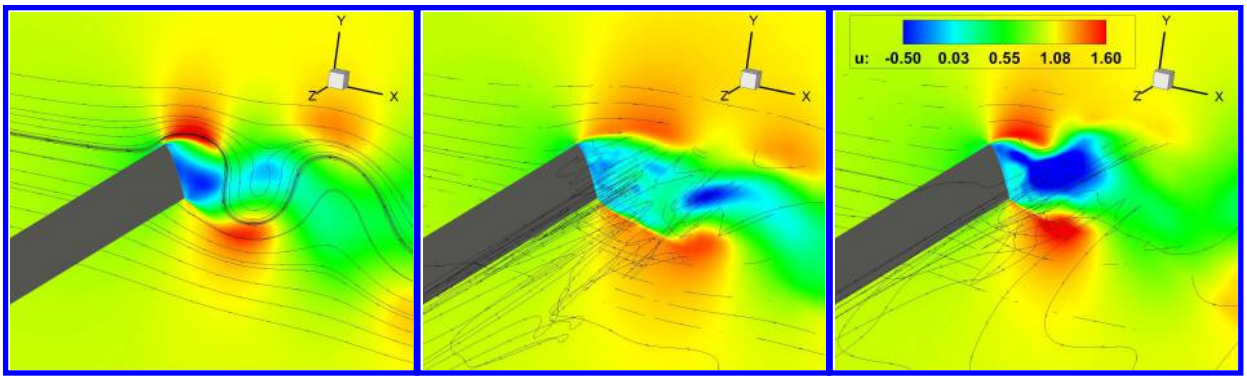

(a) URANS **(b) IDDES** **(c) SAS**

Fig. 19 Instantaneous streamlines at AoA= 60° with fine mesh

In the present study, the magnitude of vorticity is calculated based on the normalized velocity. Figs. 14 and 15 represent the vorticity magnitude at AoA= 45° and similarly Figs. 16 and 17 show the vorticity magnitude at AoA= 60° with the mesh refinement, respectively. It is observed that the hybrid turbulence model captures the small eddy flow structures in the separated flow regions due to its function as LES in those regions. The IDDES turbulence model is able to capture more smaller eddies as compared to the SAS turbulence model and thereby representing more LES like flow structure. The SAS turbulence model captures smaller eddies as compared to the URANS turbulence model in the highly separated flow region. This behavior is attributed to the resolution of the momentum carrying eddies with the length scale larger than the geometry. As the URANS turbulence model intend to model all the length scale eddies, no small scale eddies in the stalled flow region are observed. The reason for this behavior of the URANS has to do with its overly dissipative behavior which prohibits it to generate proper spectrum of turbulent scales in the massive flow separation. With the mesh refinement, a hybrid turbulence model is able to capture more smaller eddies.

Instantaneous streamlines are shown in Figs. 18 and 19 with the fine mesh at two different AoAs. It is interesting to observe that the turbulent flow structures are more like 2-D and organized with the URANS turbulence model. In reality, turbulent flow structures are 3-D and chaotic. These turbulent flow characteristics are more evident with the IDDES and SAS turbulence model in the NACA 0012 post-stall simulation.

VIII. Conclusions

This paper has demonstrated that the SAS hybrid turbulence model is able to effectively simulate massively separated turbulent flows around NACA 0012 at angle of attacks of 45° and 60°. An introduction of von Karman length scale into the SA model helps it to adjust dynamically to the flow field and provides results similar to the large eddy simulation with a massive flow separation. Apart from preserving a RANS behavior in thin shear layer, it also regains a RANS behavior in the absence of sufficient strong inflow instability or initially resolved flow which allows it to run faster in various cases as compared to the other hybrid turbulence models like DDES, IDDES.

The promising results are obtained with the SAS turbulence model in the present study under external flow applications. In the case of subsonic flat plate case, SAS predicted velocity profile and turbulent shear stress near wall in close agreement with the RANS results. The MSD problem of DES97 is not observed with the other hybrid turbulence models used in the present study. For NACA 0012 post-stall numerical investigation, SAS over-predicts the drag coefficient by 0.25 % and 2.55 % at 45° and 60°, respectively as compared to the over-prediction by approximately 24 % with the URANS at both AoA. Apart from these quantitative results, hybrid turbulence models provide more realistic turbulent flow structure in the stalled region of the airfoil as compared to the URANS.

Acknowledgments

We would like to thank the Center for Computational Science at University of Miami, Coral Gables for providing computational resources.

References

[1] Spalart, P. R., Jou, W.-H., Strelets, M., and Allmaras, S., "Comments on the Feasibility of LES for Wings, and on a Hybrid RANS/LES Approach," 1997.

[2] Spalart, P. R., and Squires, K. D., "The Status of Detached-Eddy Simulation for Bluff Bodies," *The Aerodynamics of Heavy Vehicles: Trucks, Buses, and Trains*, edited by R. McCallen, F. Browand, and J. Ross, Springer Berlin Heidelberg, Berlin, Heidelberg, 2004, pp. 29–45.

[3] Spalart, P. R., Deck, S., Shur, M. L., Squires, K. D., Strelets, M. K., and Travin, A. K., "A New Version of Detached-eddy Simulation, Resistant to Ambiguous Grid Densities," *Theoretical and Computational Fluid Dynamics*, Vol. 20, No. 3, 2006, p. 181. doi:10.1007/s00162-006-0015-0, URL https://doi.org/10.1007/s00162-006-0015-0.

[4] Chaouat, B., "The State of the Art of Hybrid RANS/LES Modeling for the Simulation of Turbulent Flows," *Flow, Turbulence and Combustion*, Vol. 99, No. 2, 2017, pp. 279–327. doi:10.1007/s10494-017-9828-8, URL https://doi.org/10.1007/s10494-017-9828-8.

[5] Menter, F. R., and Kuntz, M., "Adaptation of Eddy-Viscosity Turbulence Models to Unsteady Separated Flow Behind Vehicles," *The Aerodynamics of Heavy Vehicles: Trucks, Buses, and Trains*, edited by R. McCallen, F. Browand, and J. Ross, Springer Berlin Heidelberg, Berlin, Heidelberg, 2004, pp. 339–352.

[6] Nikitin, N. V., Nicoud, F., Wasistho, B., Squires, K. D., and Spalart, P. R., "An approach to wall modeling in large-eddy simulations," *Physics of Fluids*, Vol. 12, No. 7, 2000, pp. 1629–1632. doi:10.1063/1.870414, URL https://doi.org/10.1063/1.870414.

[7] Shur, M. L., Spalart, P. R., Strelets, M. K., and Travin, A. K., "A hybrid RANS-LES approach with delayed-DES and wall-modelled LES capabilities," *International Journal of Heat and Fluid Flow*, Vol. 29, No. 6, 2008, pp. 1638 – 1649. URL http://www.sciencedirect.com/science/article/pii/S0142727X08001203.

[8] Menter, F. R., Kuntz, M., and Bender, R., "A Scale-Adaptive Simulation Model for Turbulent Flow Predictions," Aerospace Sciences Meetings, American Institute of Aeronautics and Astronautics, 2003. doi:10.2514/6.2003-767, URL https://doi.org/10.2514/6.2003-767.

[9] Sagaut, P., Deck, S., and Terracol, M., *Multiscale and Multiresolution Approaches in Turbulence*, 2nd ed., London Imperial College Press, 2006.

[10] Menter, F. R., and Egorov, Y., "Revisiting the Turbulent Scale Equation," *IUTAM Symposium on One Hundred Years of Boundary Layer Research*, edited by G. E. A. Meier, K. R. Sreenivasan, and H.-J. Heinemann, Springer Netherlands, Dordrecht, 2006, pp. 279–290.

[11] Xu, C.-Y., Zhou, T., Wang, C.-L., and Sun, J.-H., "Applications of scale-adaptive simulation technique based on one-equation turbulence model," *Applied Mathematics and Mechanics (English Edition)*, Vol. 36, 2014, pp. 121–130. doi:10.1007/s10483-015-1898-9.

[12] Coder, J. G., "A Scale-Adaptive Variant of the Spalart-Allmaras Eddy-Viscosity Model," AIAA AVIATION Forum, American Institute of Aeronautics and Astronautics, 2015. doi:10.2514/6.2015-2462, URL https://doi.org/10.2514/6.2015-2462.

[13] Katopodes, N., *Free-Surface Flow: Environmental Fluid Mechanics*, 1st ed., Butterworth-Heinemann, 2018.

[14] Menter, F. R., and Egorov, Y., "The Scale-Adaptive Simulation Method for Unsteady Turbulent Flow Predictions. Part 1: Theory and Model Description," *Flow, Turbulence and Combustion*, Vol. 85, No. 1, 2010, pp. 113–138. doi:10.1007/s10494-010-9264-5, URL https://doi.org/10.1007/s10494-010-9264-5.

[15] Antony, J., "Time dependent calculations using multigrid, with applications to unsteady flows past airfoils and wings," Fluid Dynamics and Co-located Conferences, American Institute of Aeronautics and Astronautics, 2018. doi:10.2514/6.1991-1596, URL https://doi.org/10.2514/6.1991-1596.

[16] Zha, G., "Comparative study of upwind scheme performance for entropy condition and discontinuities," 14th Computational Fluid Dynamics Conference, American Institute of Aeronautics and Astronautics, 1999. doi:10.2514/6.1999-3348, URL https://doi.org/10.2514/6.1999-3348.

[17] Wang, B., and Zha, G., "Comparison of a Low Diffusion E-CUSP and the Roe Scheme for RANS Calculation," 46th AIAA Aerospace Sciences Meeting and Exhibit, American Institute of Aeronautics and Astronautics, 2008. doi:10.2514/6.2008-569, URL https://doi.org/10.2514/6.2008-569.

[18] Shen, Y., Zha, G., and Wang, B., "Improvement of Stability and Accuracy for Weighted Essentially Nonoscillatory Scheme," *AIAA Journal*, Vol. 47, No. 2, 2009, pp. 331–344. doi:10.2514/1.37697, URL https://doi.org/10.2514/1.37697.

[19] Shen, Y., and Zha, G., "Improvement of weighted essentially non-oscillatory schemes near discontinuities," *Computers & Fluids*, Vol. 96, 2014, pp. 1 – 9. doi:https://doi.org/10.1016/j.compfluid.2014.02.010, URL http://www.sciencedirect.com/science/article/pii/S0045793014000656.

[20] Shen, Y., and Zha, G., "Improvement of the WENO scheme smoothness estimator," *International Journal for Numerical Methods in Fluids*, Vol. 64, No. 6, 2010, pp. 653–675. doi:10.1002/fld.2168, URL https://onlinelibrary.wiley.com/doi/abs/10.1002/fld.2168.

[21] Im, H., and Zha, G., "Delayed Detached Eddy Simulation of a Stall Flow Over NACA0012 Airfoil Using High Order Schemes," Aerospace Sciences Meetings, American Institute of Aeronautics and Astronautics, 2011. doi:10.2514/6.2011-1297, URL https://doi.org/10.2514/6.2011-1297.

[22] Shen, Y., Wang, B., and Zha, G., "Implicit WENO Scheme and High Order Viscous Formulas for Compressible Flows," Fluid Dynamics and Co-located Conferences, American Institute of Aeronautics and Astronautics, 2007. doi:10.2514/6.2007-4431, URL https://doi.org/10.2514/6.2007-4431.

[23] Shur, M. L., Spalart, P. R., Strelets, M. K., and Travin, A. K., "Detached-eddy simulation of an airfoil at high angle of attack," *Engineering Turbulence Modelling and Experiments 4*, edited by W. Rodi and D. Laurence, Elsevier Science Ltd, Oxford, 1999, pp. 669 – 678. doi:https://doi.org/10.1016/B978-008043328-8/50064-3, URL http://www.sciencedirect.com/science/article/pii/B9780080433288500643.